SLAC–PUB–16979
May 2017

Generating Single-Spike Hard X-Ray Pulses with Nonlinear Bunch Compression in Free-Electron Lasers*

S. Huang[1], Y. Ding[2], Y. Feng[2], Z. Huang[2], J. Krzywinski[2],
A. A. Lutman[2], A. Marinelli[2], T. J. Maxwell[2], D. Zhu[2]
[1] Institute of Heavy Ion Physics, School of Physics, Peking University, Beijing 100871, China
[2] SLAC National Accelerator Laboratory, Menlo Park, CA 94025, USA

Submitted to Phys. Rev. Lett.

*Work supported by Department of Energy contract DE–AC02–76SF00515.

This material is based upon work supported by the U.S. Department of Energy, Office of Science, under Contract No. DE-AC02-76SF00515.

Generating Single-Spike Hard X-Ray Pulses with Nonlinear Bunch Compression in Free-Electron Lasers

S. Huang[1], Y. Ding[2],* Y. Feng[2], Z. Huang[2], J. Krzywinski[2],
A. A. Lutman[2], A. Marinelli[2], T. J. Maxwell[2], and D. Zhu[2]
[1] Institute of Heavy Ion Physics, School of Physics, Peking University, Beijing 100871, China
[2] SLAC National Accelerator Laboratory, Menlo Park, CA 94025, USA

A simple method for generating single-spike hard x-ray pulses in free-electron lasers (FELs) has been developed at the Linac Coherent Light Source (LCLS). This is realized by nonlinear bunch compression using 20-pC bunch charge, demonstrated in the hard x-ray regime at 5.6 and 9 keV, respectively. Measurements show about half of the FEL shots containing single-spike spectrum. At 5.6-keV photon energy, the single-spike shots have a mean pulse energy of about 10 μJ with 70% intensity fluctuation and the pulse full width at half maximum is evaluated to be at 200-attosecond level.

During the past few decades, great efforts have been made in generating attosecond radiation [1, 2]. These pulses offer an opportunity for studying electronic dynamics on the atomic/molecular scale [3] and is expected to inspire new breakthroughs in ultrafast sciences [4, 5]. Presently attosecond radiation pulses are generated by high-order harmonic generation (HHG) [6, 7] with photon energy up to a few hundred eV. Extending this to the keV level has wide interest, however, it is very challenging in the HHG community due to the high-harmonic cutoff, and the pulse intensity is low [8].

X-ray free-electron lasers (FELs) [9–11] provide an alternative way for generating intense ultrashort radiation pulses at the keV energy regime, and a few facilities have been successfully operated in recent years[12–15]. Nowadays most of the x-ray FELs are based on a self-amplified spontaneous emission (SASE) mechanism. In such FELs, the radiation co-propagates with the electron bunch along the FEL undulator and the initial low-power radiation source, originating from the spontaneous emission of the electron bunch, gets amplified through interaction with the electrons until the process saturates. The total radiation pulse duration is therefore determined by the bunch length, which is typically tens of femtoseconds (fs) long containing many temporal/spectral spikes. The typical single-spike width in hard x-ray SASE radiation is about 200-300 attoseconds determined by coherence length [11].

To further shorten the pulse duration down to the attosecond regime, various ideas have been proposed in the x-ray FELs. A common way is based on time slicing of the electron bunch, in which the lasing part of the electron bunch is selectively controlled by an extremely short optical laser pulse, by a slotted foil , or by a bunch tilt with subsequent orbit control [16–32]. Most of the schemes have not been experimentally demonstrated with attosecond x-ray pulses, except a recent measurement at the LCLS using a new slotted foil shows sub-fs, hard x-ray pulses [33]. Another possible way is to reduce the bunch charge dramatically (e.g., 1 pC) and directly compress the bunch to the sub-fs level [34–36]. This extreme low-charge mode ($\sim$2 orders lower than the designed FEL machines) imposes extra requirements on the electron beam diagnostics and accelerator stability. At the LCLS, a low-charge mode with 20 pC [37] has been developed with measured x-ray pulse duration of a few fs [38, 39].

In this Letter, we report experimental demonstration of generating single-spike sub-fs hard x-ray FEL pulses at the LCLS with a recently proposed nonlinear bunch compression scheme [40]. This is realized by optimizing the voltage/phase of an existing high-harmonic radio-frequency (rf) structure, through which a nonlinearly curved electron distribution in the longitudinal (time-energy) phase space is formed after bunch compression. The electron current profile is then comprised of a high-current leading peak (a horn) and a long low-current tail. As a result, the FEL process can be restricted within the leading peak and hard x-ray pulses with a single spike have been measured.

The LCLS, as sketched in Fig. 1, comprises a 135-MeV injector (not shown in the figure), a 1-km-long linac with two four-dipole chicane bunch compressors (BC1 and BC2) at 220 MeV and 5 GeV, respectively, a 132-m-long undulator line, and transport beamlines [13]. The linac includes three sections of S-band rf traveling-wave structures at 2.856 GHz (L1S, L2, and L3) and one 4th-harmonic X-band rf section (L1X). The electron bunch is longitudinally compressed by BC1 and BC2. To do this, we accelerate the electrons at an off-crest rf phase so that the electron bunch has a time-energy chirp. During passing through the chicane, the high-energy tail travels a shorter path to catch up the low-energy head so that the bunch is compressed in time. In regular FEL operation, the time-energy chirp before the compressor is expected to be linear in order to generate a uniform final current profile. This is realized by the 4th-harmonic rf structure L1X through decelerating the electron beam, which cancels the S-band rf-curvature induced nonlinear correlation [41, 42]. Accordingly, we call the harmonic structure a phase space "linearizer" in regular FEL op-

* ding@slac.stanford.edu

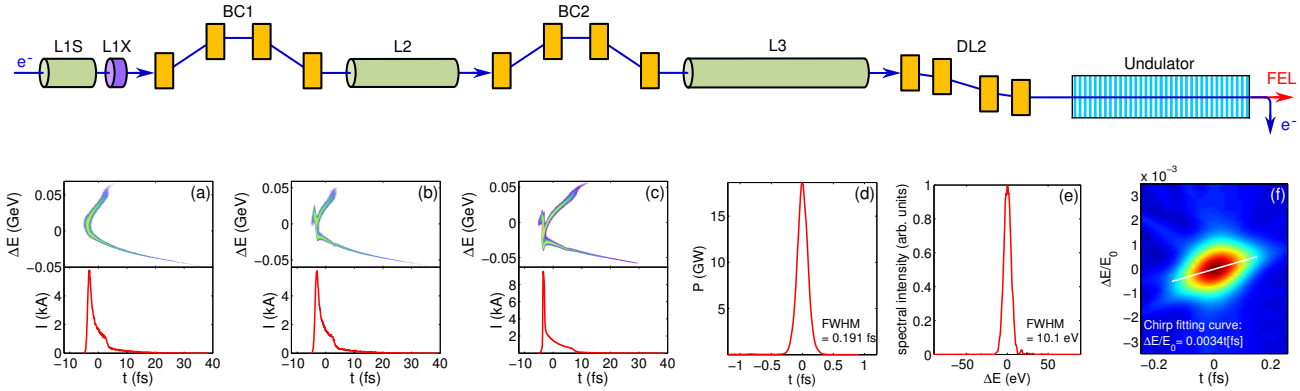

Figure 1. A sketch of nonlinear bunch compression at the LCLS. At the top is a layout of the LCLS, with main linac S-band sections (L1S, L2, L3), one X-band linac section (L1X), two bunch compressor chicanes (BC1 and BC2), a dog-leg beamline (DL2), and an undulator. The bottom plots show simulated longitudinal phase space and current profile after BC2 (a), L3 exit (b), and undulator entrance (c), and FEL simulation results, including power profile (d), spectrum (e) and Wigner transformation of the FEL field (f). The FEL photon energy in this simulation is 5.6 keV. bunch head is to the left.

eration.

In the nonlinear compression scheme, as being studied here, we intentionally reduce the amplitude of the 4th-harmonic rf structure L1X so that the electron bunch has a nonlinear time-energy chirp. During compression, we set the middle part of the bunch to get fully compressed while the head and tail would be compressed differently. As a result, a "banana"-shaped electron distribution in the longitudinal phase space will be formed after BC2, and the resultant current profile has a high-current leading peak together with a low-current tail [see Fig. 1(a)]. This distribution is similar to the early operation mode at FLASH without a linearizer [43], but here more electrons are concentrated into the middle part by optimizing the L1X parameters.

Note that some early proposals [36, 44] discussed the possibility of generating sub-fs FEL pulses from a maximum linear compression. The electron beam peak current, however, is then very sensitive to the linac rf phase jitter, which leads to a non-stable operating mode with large fluctuation of the FELs. Here one advantage of the nonlinear compression is to provide a stable current spike. As studied in [40], the linac rf phase jitter will lead to a rotation of the longitudinal phase space, but the "banana" shape is preserved. So even with rf phase jitter, we still can achieve a similar current peak but using a different part of the electron bunch. The longitudinal space charge (LSC) force downstream BC2 becomes an important factor in the system, which pushes the electrons near the horn head (tail) to higher (lower) energy. The strength of the LSC fields depends on the derivative of the electron beam current. As a result, the strong LSC force in the horn region forms a time-energy chirp with higher energy on the front, as seen in Fig. 1(b-c). Fortunately this time-energy chirp can be leveraged by reversely tapering the undulator field strength, i.e., increasing the field strength along the undulator to preserve the resonance condition of FEL [21]. We optimize the taper according to the LSC induced chirp in the beam core. Since the chirp in the core distinguishes from other parts, the taper we choose actually helps enhance lasing on the current horn and also suppress lasing elsewhere, which further shortens the x-ray pulse duration [40]. As shown in Fig. 1 (d-e), simulations predict the production of single-spike X-ray pulses with a Full Width Half Maximum (FWHM) duration around 200 attoseconds and a 10 eV FWHM bandwidth.

In the nonlinear compression experiment at the LCLS, we chose the bunch charge to be 20 pC, which has been developed for short pulse (<10 fs) operation [38]. Starting from a regular mode (linear compression, L1X voltage set at 19 MV), we only need some minor adjustments of the linac rf parameters to realize nonlinear compression. The rf amplitude of L1X was reduced first, together with L1S adjustment for maintaining the energy and current after BC1. Then we scanned the L2 phase (the L2 amplitude is adjusted accordingly with energy feedback loop to keep constant energy gain in L2) to find the minimum bunch length using the BC2 bunch length monitor [45]. By optimizing the L1X amplitude and phase we chose the best nonlinear compression setup. A list of the main LCLS parameters for nonlinear compression configuration is shown in Table *I*.

Longitudinal diagnosis of the electron beam is a critical part for carrying out this experiment. We have three longitudinal diagnostic systems available at the LCLS: a relative bunch length monitor based on coherent radiation [45], an X-band rf transverse deflector (XTCAV) [38], and a middle-infrared (MIR) prism spectrometer [46]. The relative bunch length monitor provides a quick way to know the bunch compression condition as we scan the L2 phase. When we move the phase off crest to make a time-energy chirp, the bunch length after BC2 gets shorter, and the whole bunch is still under-compressed. Increasing the chirp starts to make a maximum (full) compression on the bunch head (other parts are still under-compressed), resulting in a leading current spike. After that, a small increase of the chirp shifts

Table I. The LCLS parameters for nonlinear bunch compression experiment.

Parameter	Value	Unit
Bunch charge	20	pC
Injector bunch length	270	μm
DL1 energy	135	MeV
DL1 R56	6.3	mm
L1S rf phase	-27	degree
L1X rf phase	-170 --180	degree
L1X rf amplitude	12 - 15	MV
BC1 energy	220	MeV
BC1 R56	-45.5	mm
L2 rf phase	-35.4 - -34.8	degree
BC2 energy	5	GeV
BC2 R56	-24.7	mm
L3 rf phase	0	degree
DL2 energy	$11-14$	GeV
DL2 R56	0.133	mm

the full compression section to the bunch center, while the head is over-compressed and the tail is still under-compressed. The latter is the desired operating point with a "banana" shape. A further increase in the chirp makes the whole bunch over-compressed with the bunch head and tail switched. Operating in the longer pulse range, as in the undercompression and overcompression, it is possible to measure the time-energy phase space distribution with the XTCAV. However, the phase-space details of the electron distribution for the "banana"-shaped beam with full-compression on the core part, are beyond the resolution achievable with the XTCAV (the measured resolution with upgraded SLED mode [47] is about 2 fs rms [48] at this energy range). For this extremely short bunch, the MIR prism spectrometer provides a better resolution to guide the setup.

We show the spectral measurements with the MIR prism spectrometer in Fig. 2. This frequency-domain diagnostic is based on measuring the power spectrum of the light produced by an electron bunch undergoing a coherent transition radiation process with a thin foil. While we scan the L2 phase, the bunch length after BC2 compressor is varied and each single shot spectrum is recorded. The 2D plot shows spectral intensity distribution as a function of L2 phase and the radiation spatial frequency $\kappa \equiv 1/\lambda$ (λ is the transition radiation wavelength), where the maximum bandwidth ($\Delta\kappa$) corresponds to minimum bunch length (maximum compression). One can see the measured maximum bandwidth at the nonlinear compression mode with L1X at 12 MV is clearly larger compared to the one at linear compression (L1X at 19 MV). The electron current profile can be retrieved from the measured spectral profile by the Kramers-Kronig phase reconstruction method (see details in [46] and references there). We also show two examples of the reconstructed current profile at the maximum compression, with L1X at 12 MV and 19 MV, respectively. As we can see in Fig. 2, at nonlinear compression, the peak current is increased by about a factor 2 with bunch duration about 1 μm (3 fs) FWHM. Note that with these extremely short pulses, the measurement is still limited by instrument resolution with high-frequency content clearly extending just beyond the range of the spectrometer, and so this is still only an upper limit.

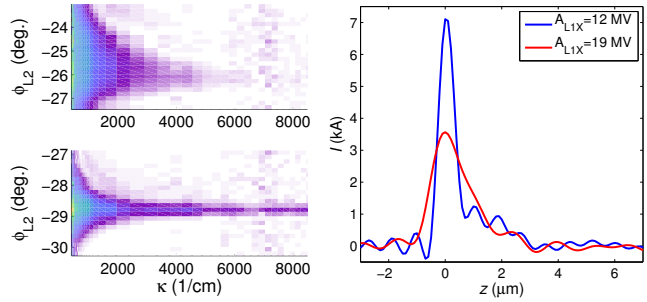

Figure 2. (Left) Spectral measurement using the MIR prism spectrometer versus L2 phase at linear (top, L1X at 19 MV) and nonlinear (bottom, L1X at 12 MV) compression. (Right) Two reconstructed current profile examples at minimum achieved pulse duration for linear and nonlinear compression. Electron beam energy was 14 GeV, bunch charge was 20 pC.

The nonlinearly compressed electron bunch was then transported to the LCLS undulator for producing x rays. As discussed earlier, the LSC induces a distinguished chirp at the beam core part. Inside the undulator, the LSC force is even stronger due to wiggling motion [49], further enhancing the time-energy chirp within the electron bunch. We applied a linear taper during the experiment of about -1% of the whole undulator to counteract this chirp effect.

Temporal characterization of these short x-ray pulses is very challenging. Instead, spectral domain diagnosis provides a possible way [50, 51]. At the LCLS, a transmissive hard x-ray single-shot spectrometer has been developed [52, 53]. Base on the Bragg reflection of a parallel incoming x-ray by a cylindrically bent silicon crystal, the spectrometer has a wide spectral range in the hard x-ray regime and a resolution at sub-eV level, which is sufficient to resolve individual SASE spectral spikes in the experiment.

Figure 3 demonstrates the FEL spectrum evolution while switching the LCLS from the regular linear compression mode to the nonlinear compression mode at the same photon energy of 9 keV. Each histogram in Fig. 3 left column was computed based on 2000 consecutive shots. We see that in the regular linear compression mode, most of the shots have 5-7 spikes. By reducing the L1X voltage to 15 MV, the number of spikes in each shot is reduced, with more than half of the shots presenting 2-3 spikes. Lowering L1X to 12 MV, we achieved most of the shots with single or double spikes as shown in the figure. The average pulse energy of the single-spike shots is about 7 μJ. If we further reduce L1X to 10 MV,

the histogram of the spike number is similar to the case at 12 MV, but the average pulse energy is reduced to 4 μJ. This means that at 10 MV, there is smaller number of electrons in the current spike due to a stronger curvature of the longitudinal phase space. For this 9-keV photon beam, we concluded that L1X at 12 MV is an optimized condition. The right column of Fig. 3 shows one typical spectrum recorded at each setting. As we can see, the number of spikes is reduced and the spike width is increased while lowering the L1X voltage. Based on statistical theory, we expect the pulses to have a similar number of spikes in time domain.

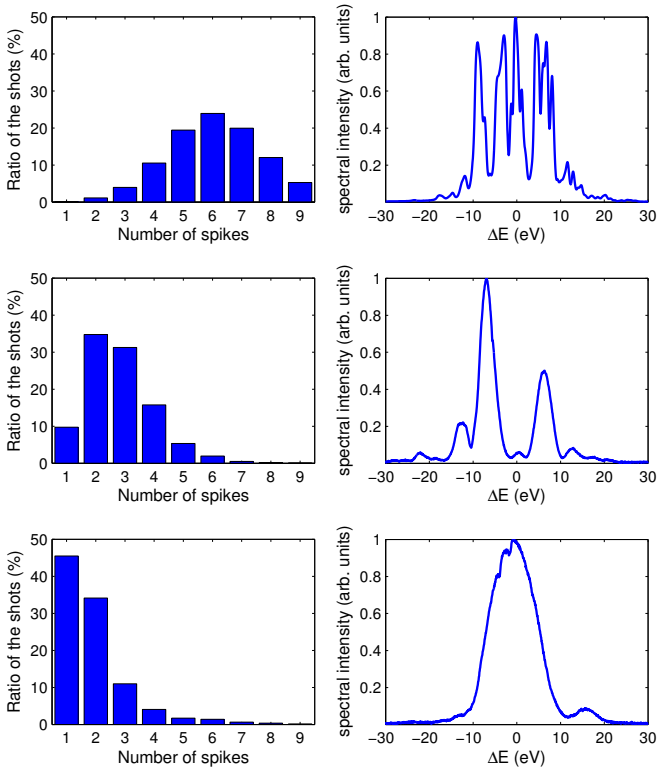

Figure 3. Histogram of the number of spikes (Left) and measured spectral example (Right) at 9 keV versus the L1X voltage: (Top) 19 MV; (Middle) 15 MV and (Bottom) 12 MV. Each setting used 2000 shots. Electron beam energy was 14 GeV, bunch charge was 20 pC.

More measurements were performed at the x-ray photon energy of 5.6 keV. After optimization, we chose the L1X at 13 MV which produces the highest ratio of single-spike pulses. In Fig. 4, we plot the histogram of the number of spikes calculated on a dataset with 8400 consecutively recorded spectra. About 50% of the shots were single spike. After sorting the shots according to the number of spikes, the average energy for the single-spike shots was about 10 μJ with 70% fluctuation. We also show 10 continuous single-spike spectral examples choosing from the sorted single-spike group. The FWHM bandwidth of these measured single-spike spectra, obtained through Gaussian fitting, was 11.3 ± 4.2 eV. Such bandwidth yields a duration of 160 ± 59 attoseconds FWHM assuming that the pulses have Fourier-transform-limited Gaus-

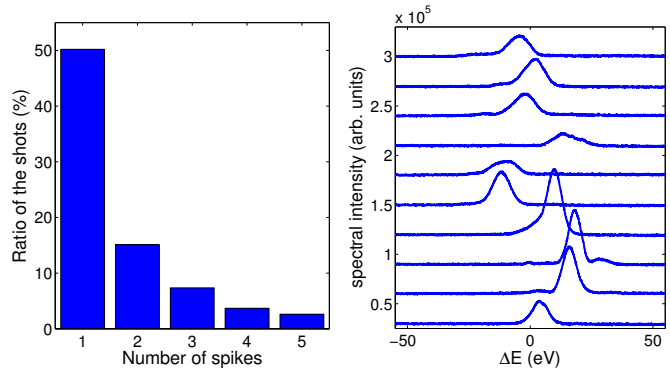

Figure 4. (Left) Histogram of the number of spectral spikes based on 8400 shots. (Right) Ten recorded shots of the sorted single-spike x-ray spectra (at 5.6 keV). Electron beam energy was 11.5 GeV, bunch charge was 20 pC. L1X amplitude was 13 MV.

sian distribution. However, as the FEL was generated by time-energy chirped electrons herein, the radiation presents a frequency chirp leading to an underestimate of the pulse length.

To derive the FEL pulse duration, a simple model for linearly chirped Gaussian pulses can be applied [54]. With this model, the FWHM pulse duration, τ_p, can be calculated using

$$\tau_p = \frac{2\sqrt{2}\ln 2/\pi}{\sqrt{\Delta f_p^2 + \sqrt{\Delta f_p^4 - (2\ln 2\,\alpha\omega_0/\pi^2)^2}}}, \qquad (1)$$

where Δf_p is the spectral FWHM, ω_0 is the central frequency, α is the frequency chirp parameter defined as the relative change of instantaneous frequency over time Δt, i.e., $\alpha = \Delta\omega/\omega_0/\Delta t$. We first apply this equation to a simulated example. A frequency chirp of 3.4×10^{-3}/fs is derived by linearly fitting the Wigner function distribution[51] shown in Fig. 1(f). Together with the simulated spectral FWHM of 10.1 eV at 5.6 keV, a FWHM pulse duration of 194 attoseconds is derived by using Eq. (1), which is consistent with the time-domain simulation result showing 191 attoseconds [see Fig. 1(d)]. An accurate measurement of the frequency chirp is unavailable in the experiment. Note that Eq. (1) has a maximum of $\tau_{p,max} = 2\sqrt{2}\ln 2/\pi/\Delta f_p$ when $\alpha = \pi^2\Delta f_p^2/(2\ln 2\,\omega_0)$, imposed by the upper limit of frequency chirp at a given spectral width. So we can estimate the upper limit of FWHM pulse duration to be 223 ± 83 attoseconds for these measured single-spike shots at 5.6 keV.

In conclusion, we have demonstrated a simple way for generating single-spike hard x-ray FEL pulses at the LCLS. At 5.6-keV photon energy, about half of the shots have single spike with estimated FWHM pulse duration at 200-attosecond level. At the LCLS, we expect to have a similar performance in a range of 4 -10 keV, and in principle this scheme should also work in soft x-ray regime. Due to a larger slippage length at soft x-ray FELs, a soft

x-ray single spike width of is expected to be about 1-2 fs. This kind of experiment can be carried out at any other x-ray FEL facilities that implement an RF linearizer, and the stability can be further improved with superconducting rf accelerators.

This work is supported by the U.S. Department of Energy Contract No. DE-AC02-76SF00515 and the National Key Research and Development Program of China (Grant No. 2016YFA0401904).

[1] G. Sansone, L. Poletto, and M. Nisoli, Nat. Photon. **5**, 655 (2011).
[2] M. Chini, K. Zhao, and Z. Chang, Nat. Photon. **8**, 178 (2014).
[3] Z. Chang and P. Corkum, J. Opt. Soc. Am. B **27**, B9 (2010).
[4] P. H. Bucksbaum, Science **317**, 766 (2007).
[5] F. Krausz and M. Ivanov, Rev. Mod. Phys. **81**, 163 (2009).
[6] X. F. Li, A. L'Huillier, M. Ferray, L. A. Lompré, and G. Mainfray, Phys. Rev. A **39**, 5751 (1989).
[7] A. McPherson, G. Gibson, H. Jara, U. Johann, T. S. Luk, I. A. McIntyre, K. Boyer, and C. K. Rhodes, J. Opt. Soc. Am. B **4**, 595 (1987).
[8] T. Popmintchev and et al., Science **336**, 1287 (2012).
[9] Z. Huang and K.-J. Kim, Phys. Rev. ST Accel. Beams **10**, 034801 (2007).
[10] B. W. J. McNeil and N. R. Thompson, Nat. Photon. **4**, 814 (2010).
[11] K.-J. Kim, Z. Huang, and R. Lindberg, "Synchrotron radiation and free-electron lasers," (Cambridge, 2017).
[12] W. Ackermann and et al., Nat. Photon. **1**, 336 (2007).
[13] P. Emma and et al., Nat. Photon. **4**, 641 (2010).
[14] T. Ishikawa and et al., Nat. Photon. **6**, 540 (2012).
[15] E. Allaria and et al., Nat. Photon. **7**, 913 (2013).
[16] E. Hemsing, G. Stupakov, D. Xiang, and A. A. Zholents, Rev. Mod. Phys. **86**, 897 (2014).
[17] E. L. Saldin, E. A. Schneidmiller, and M. V. Yurkov, Opt. Commun. **212**, 377 (2002).
[18] E. L. Saldin, E. A. Schneidmiller, and M. V. Yurkov, Opt. Commun. **237**, 153 (2004).
[19] E. L. Saldin, E. A. Schneidmiller, and M. V. Yurkov, Opt. Commun. **239**, 161 (2004).
[20] A. A. Zholents, Phys. Rev. ST Accel. Beams **8**, 040701 (2005).
[21] E. L. Saldin, E. A. Schneidmiller, and M. V. Yurkov, Phys. Rev. ST Accel. Beams **9**, 050702 (2006).
[22] A. A. Zholents and M. S. Zolotorev, New Journal of Phys. **10**, 025005 (2008).
[23] Y. Ding, Z. Huang, D. Ratner, P. Bucksbaum, and H. Merdji, Phys. Rev. ST Accel. Beams **12**, 060703 (2009).
[24] J. Qiang and J. Wu, Appl. Phys. Lett. **99**, 081101 (2011).
[25] J. Qiang and J. Wu, J. Mod. Optics **58**, 1452 (2011).
[26] P. Emma, Z. Huang, and M. Borland, Proceedings of FEL conference (FEL2004), Trieste, Italy , 333 (2005).
[27] N. R. Thompson and B. W. J. McNeil, Phys. Rev. Lett. **100**, 203901 (2008).
[28] D. J. Dunning, B. W. J. McNeil, and N. R. Thompson, Phys. Rev. Lett. **110**, 104801 (2013).
[29] T. Tanaka, Phys. Rev. Lett. **110**, 084801 (2013).
[30] E. Prat and S. Reiche, Phys. Rev. Lett. **114**, 244801 (2015).
[31] E. Prat, F. Lohl, and S. Reiche, Phys. Rev. ST Accel. Beams **18**, 100701 (2015).
[32] A. A. Lutman, T. J. Maxwell, J. P. MacArthur, M. W. Guetg, N. Berrah, R. N. Coffee, Y. Ding, Z. Huang, A. Marinelli, S. Moeller, *et al.*, Nature Photonics **10**, 745 (2016).
[33] A. Marinelli et al., to be submitted, (2017).
[34] J. B. Rosenzweig and et al., Nucl. Instrum. Meth. A **593**, 39 (2008).
[35] S. Reiche, P. Musumeci, C. Pellegrini, and J. B. Rosenzweig, Nucl. Instrum. Meth. A **593**, 45 (2008).
[36] V. Wacker and et al., Proceedings of FEL2012, Nara, Japan , 606 (2012).
[37] Y. Ding and et al., Phys. Rev. Lett. **102**, 254801 (2009).
[38] C. Behrens and et al., Nat. Commun. **5**, 3762 (2014).
[39] Y. Ding and et al., Proceedings of IPAC2013, Shanghai, China , 1316 (2013).
[40] S. Huang, Y. Ding, Z. Huang, and J. Qiang, Phys. Rev. ST Accel. Beams **17**, 120703 (2014).
[41] P. Emma, LCLS Technical Note **SLAC-TN-05-004** (2001).
[42] K. Floettmann, L. T., and P. P., TESLA-FEL-01-06, DESY-HH (2001).
[43] M. Dohlus and et al., Nucl. Instrum. Meth. A **530**, 217 (2004).
[44] L. Wang, Y. Ding, and Z. Huang, Proceedings of IPAC2011, San Sebastián, Spain , 3131 (2011).
[45] H. Loos, Proc. SPIE 8788, Advances in X-ray Free-Electron Lasers II: Instrumentation , 87780J (2013).
[46] T. J. Maxwell, C. Behrens, Y. Ding, A. S. Fisher, J. Frisch, Z. Huang, and H. Loos, Phys. Rev. Lett. **111**, 184801 (2013).
[47] J. W. Wang and et al., Proceedings of IPAC2016, Busan, Korea , 39 (2016).
[48] P. Krejcik and et al., Proceedings of IBIC2016, Barcelona, Spain , WEPG77 (2016).
[49] G. Geloni, Nucl. Instrum. Meth. A **583**, 228 (2007).
[50] L. Giannessi and et al., Phys. Rev. Lett. **106**, 144801 (2011).
[51] G. Marcus and et al., Appl. Phys. Lett. **101**, 134102 (2012).
[52] D. Zhu and et al., Applied Physics Letters **101**, 034103 (2012).
[53] D. Rich, D. Zhu, J. Turner, D. Zhang, B. Hill, and Y. Feng, Journal of synchrotron radiation **23**, 3 (2016).
[54] A. E. Siegman, "Lasers," (University Science Books, Sausalito, California, 1986).